Ocean circulation and properties in Petermann Fjord, Greenland

H. L. Johnson,[1] A. Münchow,[2] K. K. Falkner,[3] and H. Melling[4]

[1]   The floating ice shelf of Petermann glacier interacts directly with the ocean and is thought to lose at least 80% of its mass through basal melting. Based on three opportunistic ocean surveys in Petermann Fjord we describe the basic oceanography: the circulation at the fjord mouth, the hydrographic structure beneath the ice shelf, the oceanic heat delivered to the under-ice cavity, and the fate of the resulting melt water. The 1100 m deep fjord is separated from neighboring Hall Basin by a sill between 350 and 450 m deep. Fjord bottom waters are renewed by episodic spillover at the sill of Atlantic water from the Arctic. Glacial melt water appears on the northeast side of the fjord at depths between 200 m and that of the glacier's grounding line (about 500 m). The fjord circulation is fundamentally three-dimensional; satellite imagery and geostrophic calculations suggest a cyclonic gyre within the fjord mouth, with outflow on the northeast side. Tidal flows are similar in magnitude to the geostrophic flow. The oceanic heat flux into the fjord appears more than sufficient to account for the observed rate of basal melting. Cold, low-salinity water originating in the surface layer of Nares Strait in winter intrudes far under the ice. This may limit basal melting to the inland half of the shelf. The melt rate and long-term stability of Petermann ice shelf may depend on regional sea ice cover and fjord geometry, in addition to the supply of oceanic heat entering the fjord.

1.   Introduction

[2]   The recent reduction in Arctic summer sea ice cover [*Serreze et al.*, 2007; *Parkinson and Cavalieri*, 2008], the disintegration of ice shelves off northern Canada [*Copland et al.*, 2007], and the widespread acceleration of outlet glaciers in the southeast and southwest of Greenland [*Rignot and Kanagaratnam*, 2006; *Joughin et al.*, 2010] suggest that the climate of Greenland and its surroundings may be changing, with serious implications for global and regional sea level [*Shepherd and Wingham*, 2007]. In order to predict and mitigate any change, there is an urgent need to understand the mass balance of the Greenland ice sheet, and its interaction with other components of the climate system.

[3]   Petermann glacier is one of four major outlet glaciers in Greenland that have a grounding line well below sea level, terminating in a floating tongue or shelf of ice. Rapid retreat of one of these glaciers, Jakobshavn Isbrae, back to the grounding line of its ice shelf over the past decade has resulted in an acceleration of the glacial ice flux over land

[*Holland et al.*, 2008]. This has heightened concern over the vulnerability of the remaining ice shelves in the north.

[4]   *Holland et al.* [2008] suggest that the onset of the recent surging at Jakobshavn Isbrae may have been driven by higher ocean temperatures beneath the floating portion of the glacier, rather than by reduced bottom friction associated with surface meltwaters reaching the bed rock upstream [*Zwally et al.*, 2002; *Das et al.*, 2008]. Submarine melting of smaller glaciers has been shown to account for a large fraction of the mass budget at several locations [e.g., *Rignot et al.*, 2010], and accelerated melting due to changes in the ocean conditions at the outlet of tidewater glaciers is also thought to be occurring on the eastern side of Greenland, where warm subtropical waters flood the Greenland shelf [*Straneo et al.*, 2010].

[5]   Calving events visible from satellite imagery in 2001, 2008, and 2010 have drawn considerable attention to the Petermann glacier at 81°N in northwest Greenland, and the floating ice shelf in which it terminates. However, there is no evidence that either the frequency of episodic calving or the rate of glacial advance has changed markedly since observations were first recorded in the late 1800s [*Joughin et al.*, 2010; K. K. Falkner et al., Context for the recent ice island calving of Petermann Gletscher, northwest Greenland, submitted to *Eos, Transactions, American Geophysical Union*, 2010b]. Moreover, from surface accumulation, radar and satellite observations, it appears that the dominant loss term in its mass budget (80%) is ocean-driven basal melting rather than calving. Pronounced channeling in

---

[1]Department of Earth Sciences, University of Oxford, Oxford, UK.
[2]College of Earth, Ocean and Environment, University of Delaware, Newark, Delaware, USA.
[3]College of Oceanic and Atmospheric Sciences, Oregon State University, Corvallis, Oregon, USA.
[4]Institute of Ocean Sciences, Department of Fisheries and Oceans, Sidney, British Columbia, Canada.
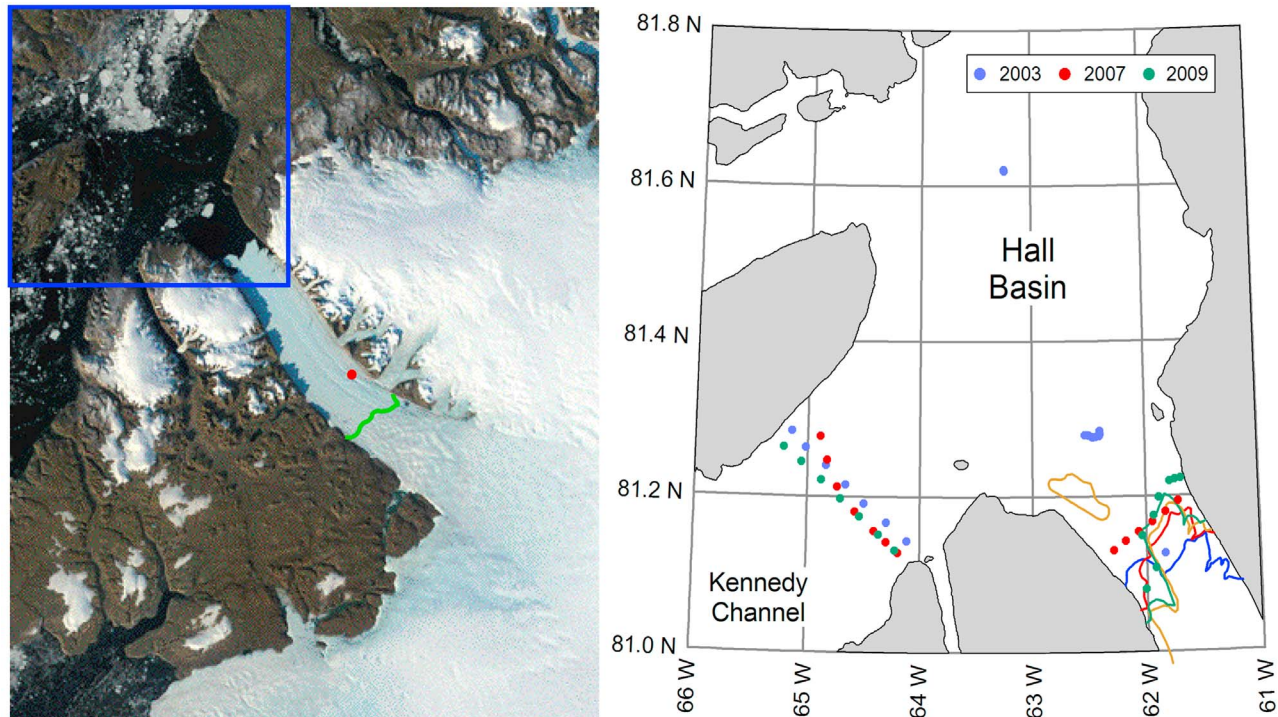
Figure 1. (left) MODIS image of Petermann Glacier and Fjord, 10 September 2003. Superimposed are the approximate positions of the glacier's grounding line and the through-ice CTD profiles, based on *Rignot and Steffen* [2008]. (right) Positions of hydrographic profiles measured by CTD from ships in 2003, 2007, and 2009. The domain of this map is outlined in blue on the MODIS image.

under-ice topography [*Rignot and Steffen*, 2008] has led glaciologists to conclude that ice shelves such as Petermann may be particularly sensitive to any future warming of ocean waters in the vicinity.

[6] Few oceanographic observations are available to constrain the properties and circulation in Petermann Fjord, and their relation to the adjacent Nares Strait. Even the depth of the sill at the mouth of the fjord is incompletely known since few soundings have ever been taken in the vicinity. In this paper we present oceanographic data collected during three opportunistic sampling efforts in the vicinity of the floating tongue of Petermann glacier in 2003, 2007, and 2009. Our aim is to discuss what can be inferred from this data about the circulation in the fjord mouth and the water mass properties beneath the floating ice shelf. We assess the amount of heat available to melt the ice shelf from below, and discuss the fate of the resulting melt water. We emphasize here that this is not a paper about secular change in the area, and does not stem from a targeted observational campaign. Nevertheless, we hope that it may provide the understanding and baseline measurements required to recognize future change in the mass balance of Petermann glacier should it occur.

2. Data

[7] Figure 1 (left) shows Petermann glacier in northwest Greenland at approximately 81°N and 61°W. The glacier flows from southeast to northwest into steep walled Petermann Fjord at about 1 km yr^{-1}. Beyond its grounding line (approximate location marked, based on *Rignot and Steffen* [2008]) it forms a floating ice tongue which, when our observations were made, was approximately 70 km long and 20 km wide, thinning from 600 m at the grounding line to approximately 60 m at its front [*Higgins*, 1991]. Petermann Fjord narrows to about 15 km close to the glacier front, and then opens out into Hall Basin in Nares Strait, which is connected to the Arctic Ocean to the north and Baffin Bay to the south.

[8] The oceanographic measurements reported here were made during summertime 1 day surveys from the US Coast Guard Cutter *Healy* (2003) and the Canadian Coast Guard Ship *Henry Larsen* (2007, 2009) during the Canadian Arctic Throughflow Study (CATS). The principle aim of CATS was to measure and understand the oceanic volume and fresh water flux from the Arctic Ocean to Baffin Bay (and hence the North Atlantic Ocean) via Nares Strait. As such, the oceanography of the wider region has been well characterized [*Münchow et al.*, 2006, 2007; *Münchow and Melling*, 2008; *Melling et al.*, 2008; *Rabe et al.*, 2010; K. K. Falkner et al., Interannual variability of dissolved nutrients in the Canadian Archipelago and Baffin Bay with implications for freshwater flux, submitted to *Deep Sea Research*, 2010a]. Figure 1 (right) shows the location of conductivity, temperature and depth (CTD) profiles discussed in the text.

[9] Figure 2 (left) shows the approximate location of the ice front during summer in 2003, 2007, 2008, and 2009.
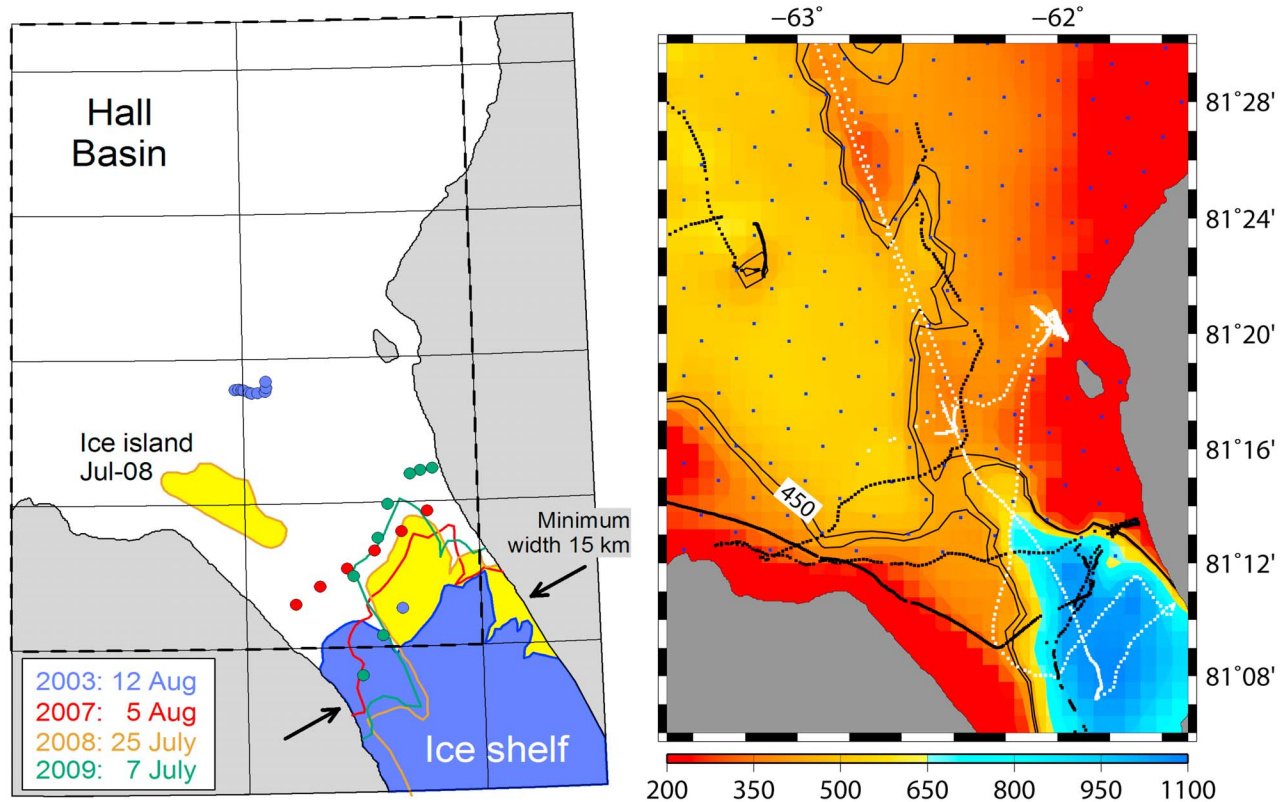
Figure 2. (left) Positions of the ice shelf front on selected dates during 2003–2009. The large island that broke free early in July 2008 is seen near the fjord mouth later in that month. The dashed polygon depicts the domain of the bathymetric map in Figure 2 (right). (right) Bathymetry in the mouth of Petermann Fjord, based on an interpolation of IBCAO data outside the fjord (blue dots) together with echo sounder data from the CCGS *Henry Larsen* (2009, black dots) and the center beam of the USCGC *Healy*'s Sea-Beam-2112 swath mapping sonar (2003, white dots). Note that IBCAO data within the fjord has not been incorporated since this is based on only one sounding. Contours are plotted at 425 and 450 m.

Note the seaward advance by 4.5 km between 2003 and 2007, equivalent to 3.1 m d^{-1} or 1130 m yr^{-1}, which is close to the average measured by remote sensing [*Rignot and Steffen*, 2008] implying negligible calving in the intervening period. A large (3.5 km by 10 km) tabular iceberg did calve in July 2008, and was subsequently tracked for almost a year as it made its way south through Nares Strait and then along the coast of Baffin Island. Measurements made by an ice-profiling sonar moored in Nares Strait captured this iceberg as it drifted overhead. The sonar data suggest a mean draft of 56 m, corresponding to a mean thickness of approximately 63 m. Maximum draft was 62 m, corresponding to a maximum thickness of approximately 69 m. The outline of this iceberg appears near the mouth of the fjord in Figure 2 (left). In August 2010 Petermann glacier lost about one fifth of its floating ice tongue in a major calving event which produced an ice island of area 253 ± 17 km^2 (Falkner et al., submitted manuscript, 2010b). This event is discussed briefly in section 7.

[10] The bottom bathymetry is shown in Figure 2 (right). Due to the lack of prior soundings in the fjord our knowledge of the bathymetry is based solely on ship track echo sounder data. These data reveal that the at least 1100 m deep fjord is separated from Nares Strait by a sill no deeper than about 450 m. Hydrographic constraints on the actual depth of the sill will be discussed in section 3. Note that Nares Strait is in turn separated from the deeper Arctic Ocean by a sill of depth 290 m near 84°N, and from deeper Baffin Bay by a southern sill of depth 220 m near 80°N [*Melling et al.*, 2001]. Hall Basin adjacent to the fjord mouth reaches depths of 800 m.

[11] The USCGC *Healy* was equipped with a 75 kHz acoustic doppler current profiler (ADCP) which enabled us to profile ocean currents from 25 m below the hull to about 350 m depth. Other available data from 2003 include a single vertical profile of water properties at the front of the glacier (and in the adjacent Hall Basin) from the surface to the bottom, sampling a range of geochemical tracers, and a sequence of 10 vertical CTD and dissolved oxygen profiles taken at 15 minute intervals near the sill of the fjord. A tracer hydrographic section was also conducted across Nares Strait just south of Petermann Fjord. In 2007 and 2009 from the CCGS *Henry Larsen*, CTD sections to a depth of approximately 500 m were completed across the fjord between the glacier front and the sill. CTD sections were also conducted across Nares Strait. In 2009, surface water
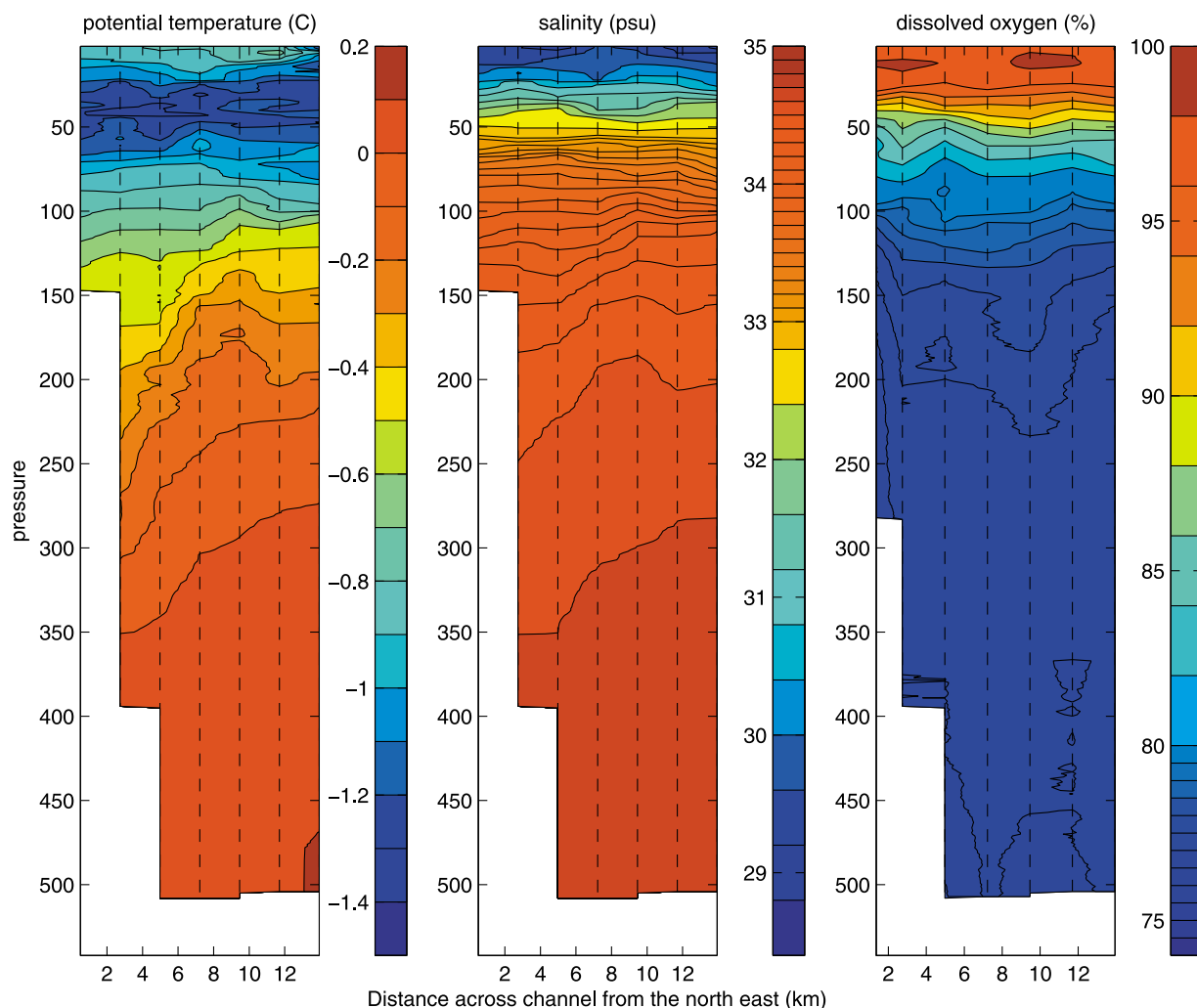
Figure 3. Sections of (left) potential temperature, (middle) salinity, and (right) dissolved oxygen across Petermann Fjord in 2009. The data are plotted looking into the fjord, with the NE wall of the fjord on the left (at 0 km) and the SW wall on the right (at approximately 16 km). The CTD data have been interpolated onto a regular grid (indicated by the vertical dashed lines) and projected onto a straight line perpendicular to the axis of the fjord before plotting. In Figure 3 (left) the contour interval is 0.1°C. In Figure 3 (middle), contours are plotted every 0.4 psu at salinities less than 33 psu and every 0.1 psu at salinities above. In Figure 3 (right) the contour interval is 2% above 80% and 0.5% below.

properties (at a depth of 1–2 m) in the fjord were sampled via a 6 h towed CTD survey from the CCGS *Henry Larsen*'s fast response craft (FRC) across the fjord close to the ice front. We also consider a CTD profile obtained through the ice shelf by *Rignot and Steffen* [2008] in 2002, at a location approximately 15 km downstream of the grounding line on the northeastern side of the fjord (see Figure 1).

3. Hydrography

[12] Sections of potential temperature, salinity, and dissolved oxygen down to 500 db across the fjord in 2009 are shown in Figure 3. The data have been interpolated onto a regular grid with a horizontal resolution of 2.25 km, and projected onto a vertical plane perpendicular to the axis of the fjord (i.e., assuming no variation in the along-fjord direction) before plotting. Typical of Arctic regions, a cold,

fresh water mass overlies a warmer, saltier, modified Atlantic water mass. The density field is not shown but looks very similar to the salinity field, with σ_t ranging from 23.1 kg m^{-3} at the surface to 27.9 kg m^{-3} at 500 db. Below about 100 db, isotherms and isohalines slope across the fjord, with colder fresher water on the northeastern side. Similar across-strait gradients were observed in 2007 (not shown). The water close to the northeastern side of the fjord at these depths is also slightly depleted in dissolved oxygen relative to the center of the fjord. The coldest water on the section lies at approximately 50 db depth on the northeastern side, although at −1.4°C this is well above the freezing temperature. There is heat available throughout the water column to melt ice, with temperatures several degrees above the freezing point at depths greater than 200 db. The surface salinity is approximately 29 practical salinity units
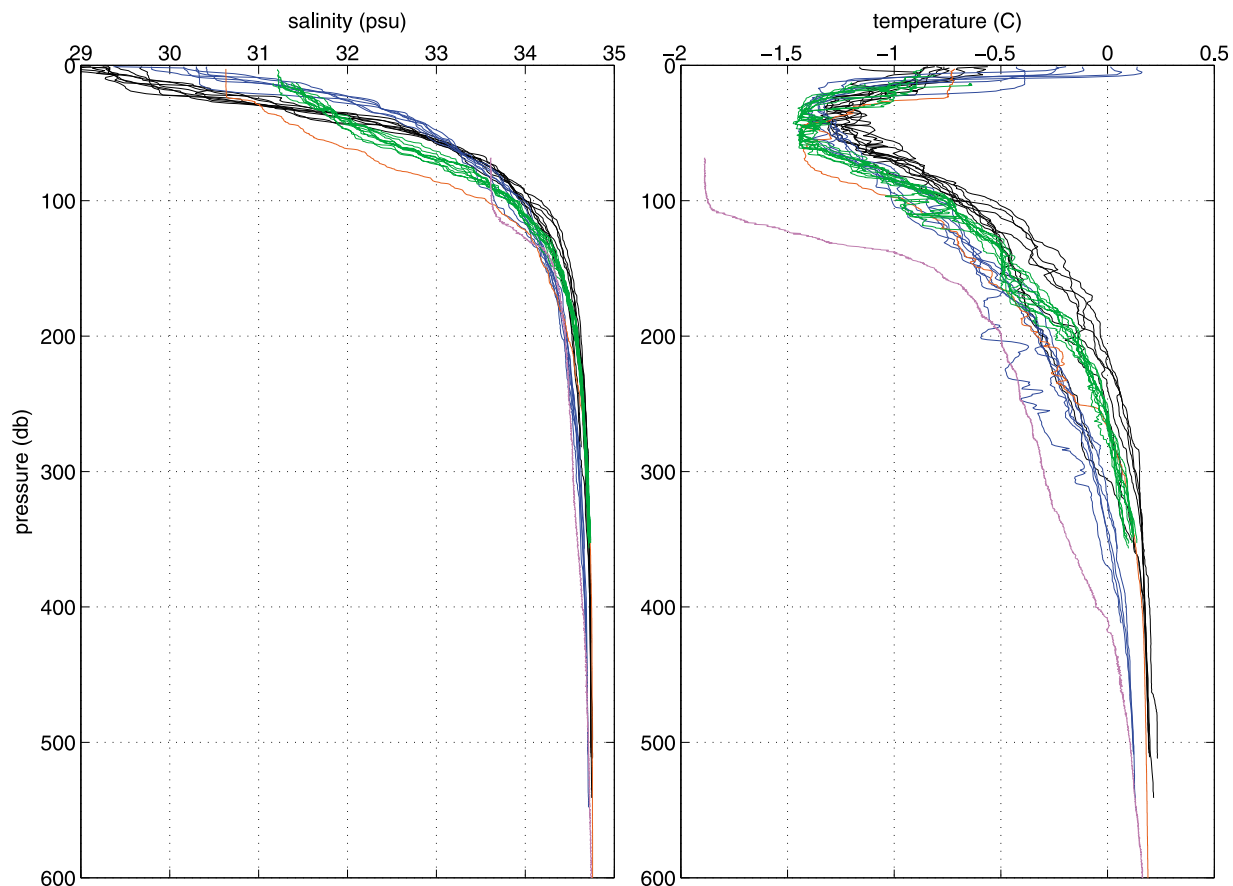
Figure 4. Vertical profiles of temperature and salinity measured in Petermann Fjord over the three surveys. The 2003 cast in the center of the fjord is shown in red, the data collected close to the sill in 2003 are shown in green, the 2007 CTD section is plotted in blue, and the 2009 CTD section is plotted in black. Shown in magenta are vertical profiles of temperature and salinity measured beneath the ice shelf approximately 15 km downstream of the grounding line in 2002 by *Rignot and Steffen* [2008] (see Figure 1 for location).

(psu), which was typical of surface water in Nares Strait at the time.

[13] Below approximately 400 db, properties in the fjord are more homogeneous (see Figure 4) and distinct from those at an equivalent depth in neighboring Hall Basin. This indicates that the fjord has been filled to sill depth by water from a narrow range of depths in adjacent Nares Strait, that lie close to the maximum depth of the sill. Tracer constraints on the ventilation of the deeper waters in the fjord are discussed in section 5. The sill depth can be estimated from water properties on either side of the sill, using the method first applied by Nansen to deduce the existence and elevation of the Lomonosov ridge from hydrographic data before it was mapped. Bottom water in Hall Basin has a salinity and potential temperature of 34.802 psu and 0.210°C, respectively. Bottom water near the ice shelf front in Petermann Fjord reaches only 34.765 psu and 0.175°C. In fact, 300 m or more above the bottom at 750 db this water is fresher by only 0.005 psu and cooler by only 0.007°C. Water with the same salinity and potential temperature found at the seabed in the fjord occurs at 387 db in Hall Basin. Provided that properties at these depths are relatively constant, the corresponding depth (383 m) might be con-

sidered the effective sill depth from the viewpoint of inflow. The actual depth is likely smaller because there are plausible dynamical mechanisms that could lift deeper water up and over the sill.

[14] Figure 5a shows the θ-S relationship at each of the CTD stations along the 2009 section. Below a depth of about 185 m (at a salinity of 34.5 psu) the θ-S curves at stations within a couple of kilometers of the northeastern wall (casts 2 and 3; note that cast 1 only reached a depth of 150 m) exhibit a slope of 2.5 °C/psu. When glacial ice melts from below, the latent heat of melting must be extracted from sea water. A consideration of the heat and salt budgets during this melting process [*Gade*, 1979] demonstrates that melted glacial ice will blend with sea water to form products that lie along a mixing line with a slope of approximately 2.5 °C/psu (for Atlantic-derived water with a temperature of 0.19°C and a salinity of 34.76 psu, such as we see at the depth of the glacier's grounding line in our 2003 CTD data).

[15] Above 185 m, and away from the northeastern side of the fjord, the θ-S curves have a shallower slope, indicating that Atlantic-derived water is mixing with fresh water without providing the necessary latent heat to accomplish melting, i.e., freshwater that has not resulted from interac-
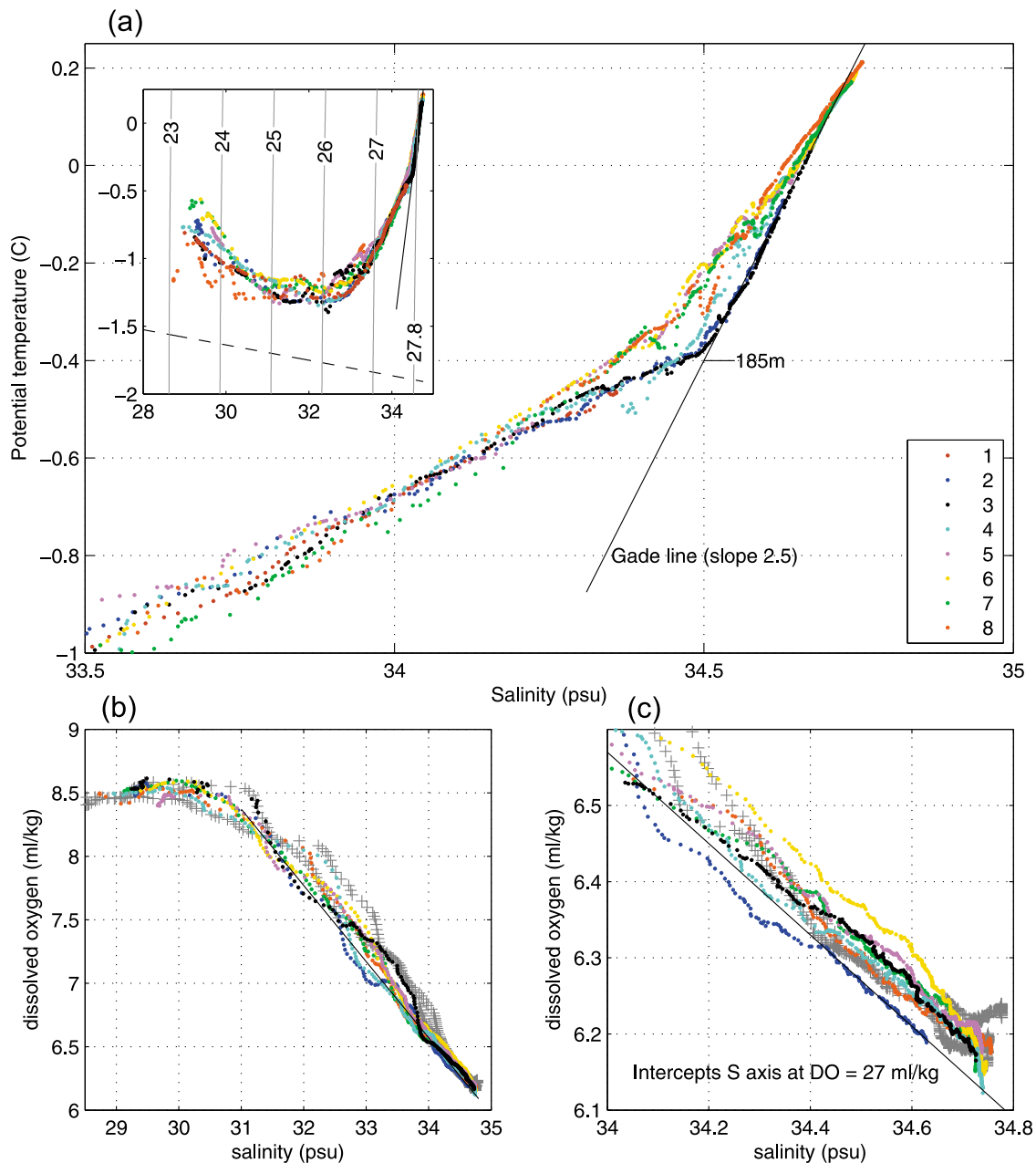
Figure 5. Property diagrams of data from a CTD section across Petermann Fjord (2009) plotted in θ-S and O$_2$-S space. Casts are numbered from the northeastern side of the fjord. The inset in Figure 5a shows the full range of the data, with the freezing line at zero pressure and contours of density (σ_t in kg m^{-3}) added. The data plotted as grey crosses in the Figures 5b and 5c are from two casts lying on a section across Nares Strait, south of the entrance to Petermann Fjord.

tion between the ocean and ice underneath the ice shelf. Possible sources of this fresh water include surface glacial melt, sea ice melt and terrestrial runoff. Note that the mixing need not have occurred in the fjord, with upper water column θ-S structure likely representative of the wider region (see the θ-S curves in Hall Basin and Nares Strait plotted in Figure 12), and arising in part due to mixing in the Arctic Ocean.

[16] Figures 5b and 5c show the correlation between salinity and dissolved oxygen for each of the 2009 Petermann Fjord CTD casts. In water with salinity less than 31 psu (above 30–40 m depth), the concentration of dissolved oxygen is relatively constant at 8.5 ml/kg, a value typical of water derived from ice melting at the sea surface, where air-sea exchange limits dissolved gas concentrations to saturation values. In water with salinity greater than 34 psu (depths greater than about 100 m), the concentrations of dissolved oxygen are consistent with a mixing of local Atlantic water with fresh water containing 27 ml/kg dissolved oxygen. This could be evidence that warm seawater at depths below 100 m has caused melting from the underside of the ice shelf where all released air bubbles must
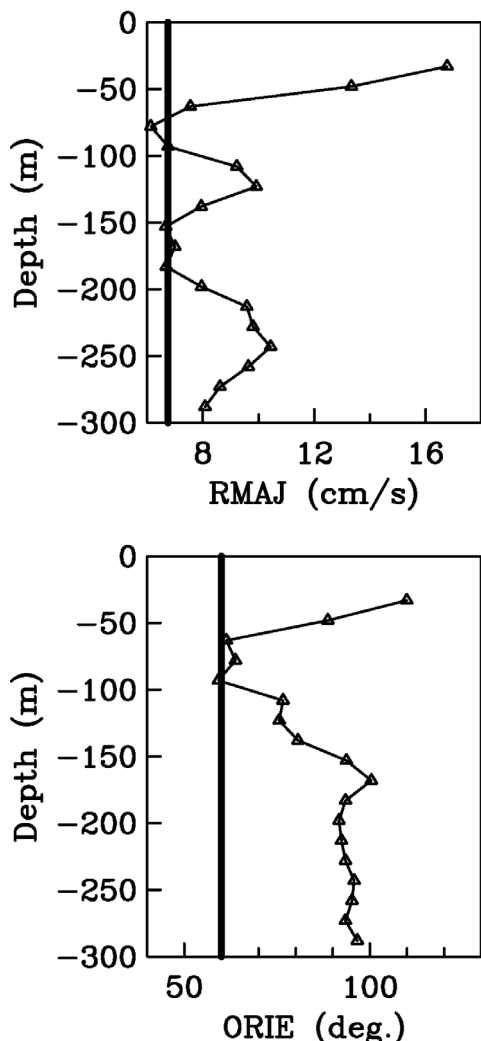
Figure 6. Vertical profile of the mean semidiurnal tidal current strength and its orientation in Petermann Fjord, based on an 18 h shipboard ADCP survey from the USCGC *Healy*. The heavy solid lines indicate tidal predictions from the *Padman and Erofeeva* [2004] barotropic tidal model, which has been sampled at the same locations and times as the data and then subjected to the same single-component harmonic analysis.

dissolve into the seawater under pressure. For salinities between 31 and 34 psu the mean slope is similar to that in the deeper waters, but there is considerable structure. Note that there may be other mechanisms in play with respect to dissolved oxygen; data from Nares Strait outside the fjord exhibit similar characteristics (see the two casts plotted as grey crosses) suggesting that these may reflect regional hydrography rather than local ocean interaction with glacial ice within the fjord. Hence, dissolved oxygen alone is not an unambiguous indicator of subsurface glacial melt water in Petermann Fjord.

[17] The θ-S curves for all of the CTD data collected in Petermann Fjord over the three snapshot surveys (together with data collected through the ice close to the grounding line by *Rignot and Steffen* [2008]) are shown in Figure 12 and will be discussed in section 7. The variability in space and time illustrates that our snapshots of the hydrographic structure in Petermann Fjord are unlikely to be representative of the long-term mean, and that the interannual differences apparent here are not indicative of a trend.

4. Circulation

4.1. Tides

[18] Moored ADCP data have shown that over 90% of the ocean current variance in Nares Strait occurs at tidal frequencies [*Münchow and Melling*, 2008]. Model predictions of tidal currents may vary substantially from actual tidal currents, particularly inside Petermann Fjord, on account of the poorly resolved bottom bathymetry [*Padman and Erofeeva*, 2004; [*Münchow et al.*, 2006]. Here we estimate tidal currents from 18 h of shipboard ADCP measurements made from the USCGC *Healy* in 2003. To make best use of our short data set, we assume that the tide is entirely semidiurnal, and is uniform along our ship track within the fjord (see Figure 2). We use the method of least squares to estimate the mean eastward(u_1) and northward (u_2) components of the tide as a function of depth, by fitting all observations to the function $u_i(z) = a_i(z) * \cos\omega t + b_i(z)\sin\omega t$, with $i = 1,2$ and where $\omega = \frac{2\pi}{T}$ is the M2 tidal frequency which has a period T of 12.42 h.

[19] Figure 6 shows the magnitude and direction of the tidal current, calculated from the empirically determined amplitudes $a_i(z)$ and $b_i(z)$. The amplitude of variability at semidiurnal frequencies is of order 10 cm s^{-1}, which is considerably smaller than semidiurnal tidal currents as large as 24 cm s^{-1} in Nares Strait [*Münchow and Melling*, 2008]. The amplitude decreases by a factor of 2 from 0.16 m s^{-1} at 30 m depth to 0.08 m s^{-1} at 100 m depth, with concurrent variation in orientation. This variation with depth may relate to the strong stratification in the upper part of the water column and/or the presence of inertial oscillations which, at this latitude, have a period close to 12.14 h. Petermann Fjord, at 81°N, is well above the critical latitude for the M2 tide (74.5°N) so that density anomalies generated by interaction of the barotropic tide with the sill are unlikely to propagate as internal waves, with the energy instead channeled into localized, near-inertial motions.

[20] The heavy solid lines in Figure 6 indicate the results of the same harmonic, single-constituent analysis applied to tidal current predictions from a barotropic model with 8 tidal constituents [*Padman and Erofeeva*, 2004], at the same locations and times as the USCGC *Healy* (2003) ADCP data were sampled. The result lies close to the vertical average of the data, although does not capture the surface intensification. Further analysis of the tidal model (not shown) suggests that the maximum amplitude in tidal current at the mouth of Petermann Fjord is a factor of approximately 1.2 larger than that during our survey.

[21] As well as tidal current, the tidal range is also important to the dynamics and water mass properties in Petermann Fjord, since it influences the flexing of the ice sheet and the forcing of the under-ice cavity. The nearest reference data for tidal range is from Polaris Bay (75°22′N, 96°51′W) in 1871 (0.547 and 0.123 m for M2 and K1, respectively, with an estimated range of 2.38 m [*Bessels*,
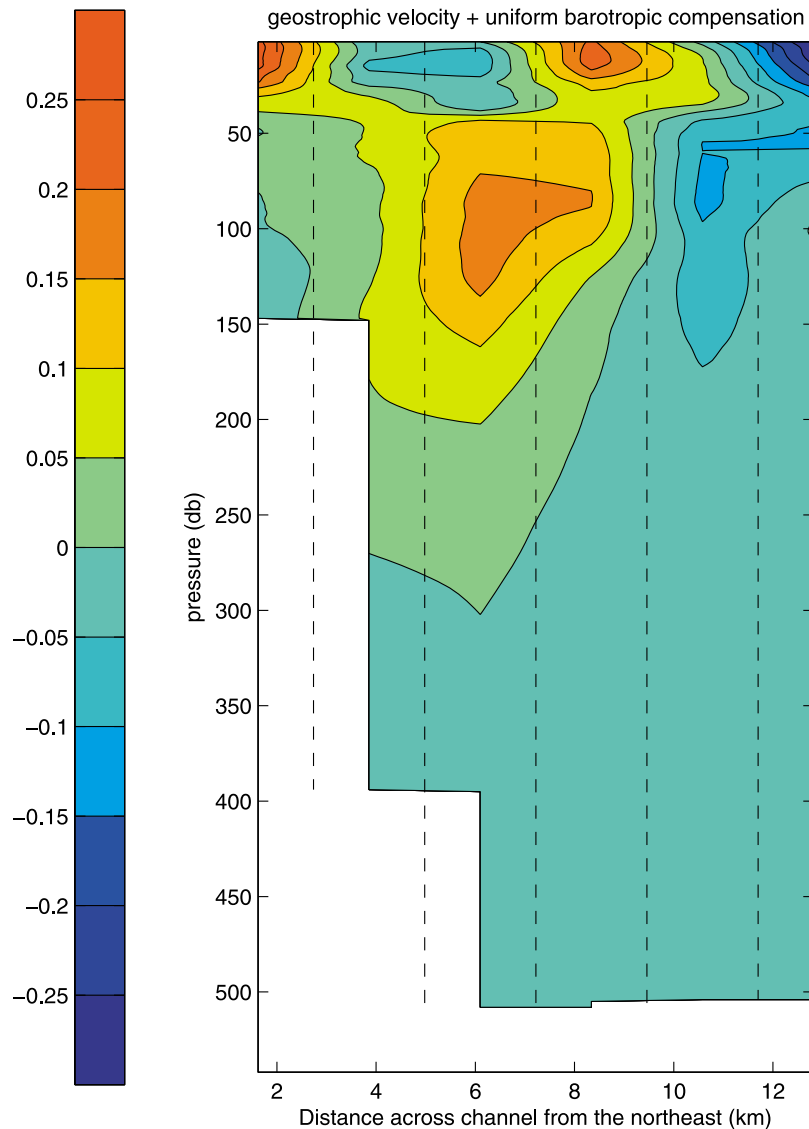
Figure 7. Geostrophic velocity (m s^{-1}) based on the 2009 hydrographic section across the fjord. A uniform compensating velocity (-3.2 cm s^{-1}) has been added over the cross-sectional area spanned by the data to ensure zero net flux. The data are plotted looking into the fjord, with the NE wall of the fjord on the left (at 0 km) and the SW wall on the right (at approximately 16 km). Positive velocities are directed out of the fjord. The CTD data were interpolated onto a regular grid (indicated by the vertical dashed lines) before calculating geostrophic velocities. Note that during the 2009 survey the ice shelf protruded further on the north east side of the fjord than the south west (see Figure 11), with the transition occurring at approximately 9 km across the fjord.

1876]) and Cape Defosse (81°14′N, 65°36′W) in 1985 (0.759, 0.345, 0.169, and 0.093 m for M2, S2, N2, and K2, respectively; 0.152, 0.052, and 0.050 m for K1, O1, and P1, respectively, with a range of 3.24 m).

[22] In summary, the tidal energy within Petermann Fjord is considerably diminished from that in Nares Strait, and is largest in the upper portion of the water column. Since tides are, in general, a potential source of kinetic energy for mixing under the ice shelf, this has implications for the detailed ice-ocean interaction processes that govern basal melting.

4.2. Geostrophic Flow

[23] Figure 7 shows the geostrophic velocity field determined from the hydrographic section in Figure 3. The velocity is positive when directed out of the fjord (and out of the page). A uniform barotropic velocity has been added across the section (approximately -3 cm s^{-1}) to ensure that there is no net flow into the fjord above 500 m. (Note that this is an approximation since (1) the fjord extends to greater depth and (2) there is, in fact, a small net volume flux out of the fjord equal to the amount of freshwater that crosses the
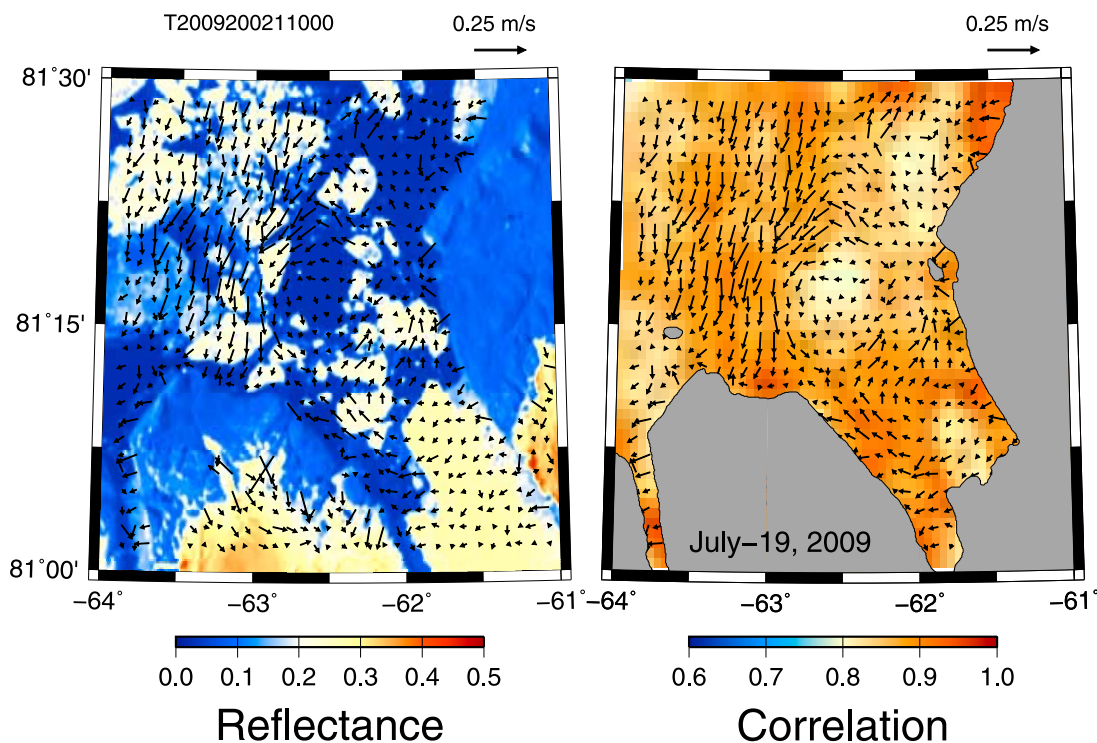
Figure 8. Average surface velocity calculated from correlations of a series of eight sequential MODIS-Terra images (645 nm wavelength, 250 m resolution) between 1435 UTC on 19 July 2009 and 0205 UTC on 20 July 2009. Figure 8 (left) also shows reflectance at 2110 UTC on 19 July 2009, while Figure 8 (right) shows the maximum correlation for each grid point, averaged over the image sequence.

grounding line as ice and melts before reaching the glacier front; see section 7.) The internal deformation radius is of order 5–10 km, significantly narrower than the fjord width (about 16 km) at this point.

[24] Below 50 m there is a geostrophic flow out of the fjord within 9 km of the northeastern wall, with velocities reaching a maximum value of almost 20 cm s^{-1} at a depth of 100 m. This flow is compensated by a net volume flux into the fjord on the southwestern side, which extends all the way to the surface. The geostrophic velocity field in the upper 50 m exhibits a complex structure, with several reversals in flow direction across the width of the strait. Note that close to the surface and to the fjord walls we do not expect the flow to be in geostrophic balance due to the importance of friction and wind forcing. The geostrophic velocity field in 2007 was similar, although the velocities were weaker.

[25] Note that during (and for the 2 days preceding) our 2009 survey in Petermann fjord the wind was directed out of the fjord. One might therefore expect the surface Ekman circulation to depress isopycnals on the northeastern side of the fjord, and generate an outward geostrophic current there. However, this circulation will only become established after one or more inertial periods of drift from the ice front, well beyond the location of our section. The discontinuity in surface stress at the ice front will also promote a local (nonrotational) upwelling response which may influence the hydrography observed and the properties of the water flowing out of the fjord.

4.3. Surface Circulation Inferred From Remote Sensing Data

[26] Under suitable conditions, surface circulation can be estimated from a sequence of MODIS images. Figure 8 shows a map of motion vectors generated by considering cross correlations (averaged over 1 km^2) between a series of eight sequential MODIS-Terra images for 19 July 2009. The 645 nm wavelength (red) band was used; images have a spatial resolution of 250 m and are separated in time by approximately 90 minutes. Figure 8 (left) shows reflectance at 2110 UTC on 19 July 2009. Figure 8 (right) shows the maximum correlation for each grid point, averaged over time. Stationary features with high contrast, such as Petermann glacier's front, show particularly high correlations. Note that the World Vector Shoreline (superimposed) has the ice front in the wrong location for this time period. Vectors over glacial ice on land or water may be interpreted as the magnitude of uncertainty due to noise.

[27] There is a cyclonic gyre in the mouth of Petermann Fjord, with velocities similar in magnitude to the geostrophic velocities in Figure 7. Note also the strong surface outflow on the southwestern wall of the fjord that crosses over to the northeastern wall near the fjord mouth. The general southward flow from the north into Kennedy Channel is shown in the top left corner of the frame, and appears to also have a cross-strait component. While the inferred surface circulation may still contain a tidal bias, a similar flow pattern at the mouth of the fjord also emerges from ENVISAT synthetic aperture radar data for the same
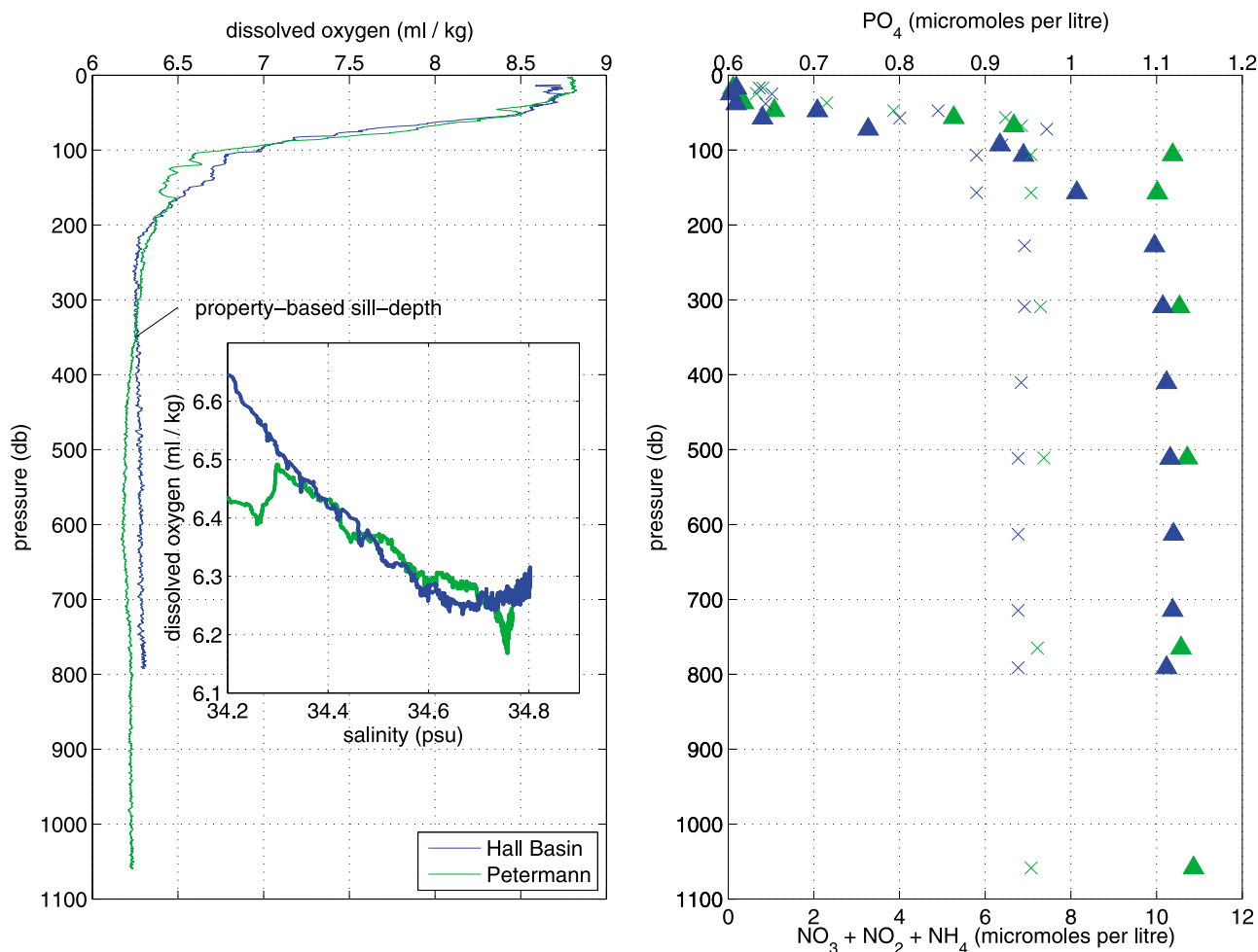
Figure 9. Vertical profiles of dissolved oxygen and nutrients for the center of Petermann Fjord and for Hall Basin in 2003. Petermann Fjord data are plotted in green and Hall Basin data in blue. In Figure 9 (right), nitrate ($NO_2 + NO_3 + NH_4$) is plotted as triangles, while phosphate (PO_4) is plotted as crosses. The inset of Figure 9 (left) shows the O_2-S relationships. Note the negative dissolved oxygen excursion in Petermann Fjord at a salinity of 34.76, below which the O_2 increases with depth toward the O_2-S relationship on the Hall Basin side of the sill. Note also that nutrient concentrations in a similar depth range are higher in Petermann Fjord than Hall Basin.

period (P. Gudmandsen, personal communication, 2010). A strong cyclonic circulation at the mouth of the fjord is often evident in MODIS imagery at other times during the mobile sea ice season (not shown).

5. Tracer Hydrography

[28] Chlorofluorocarbon (CFC) data in Hall Basin immediately outside Petermann Fjord suggest that waters deeper than the 290 m sill depth to the north are ventilated on a timescale of about 30 years (not shown). Over this time the dissolved oxygen content of the water falls to about 80% of surface saturation values. Equivalent CFC data are unfortunately not available for Petermann Fjord. However, silicate, nitrate and phosphate concentrations below sill depth are slightly higher than those in Hall Basin at an equivalent salinity, while oxygen concentrations are lower (see Figure 9), suggesting that the deep waters of Petermann

Fjord are ventilated on a timescale somewhat longer than 30 years.

[29] In fact, the vertical profile of oxygen concentrations in Petermann Fjord shows a distinct minimum at depths of 500–600 m. Nitrate and phosphate are enhanced at the same depths, with the differences small but in Redfield proportions. Within this depth range the θ-S curve from the same CTD cast shows interleaving of water masses, some of which lie along a Gade-like slope (see Figure 12). Below this depth the oxygen concentration increases with depth toward the dissolved oxygen-salinity relationship on the Hall Basin side of the sill. This indicates that the bottom waters in the fjord are renewed by spillover at the sill (which, from a dissolved oxygen perspective, appears to have a depth of approximately 350 m; see Figure 9) while the waters at about the depth of the grounding line appear "older", with a stronger nutrient regeneration imprint.

[30] Plotted in Figure 10 is the relationship between $\delta^{18}O$ and salinity in the upper 100 m of the water column close to
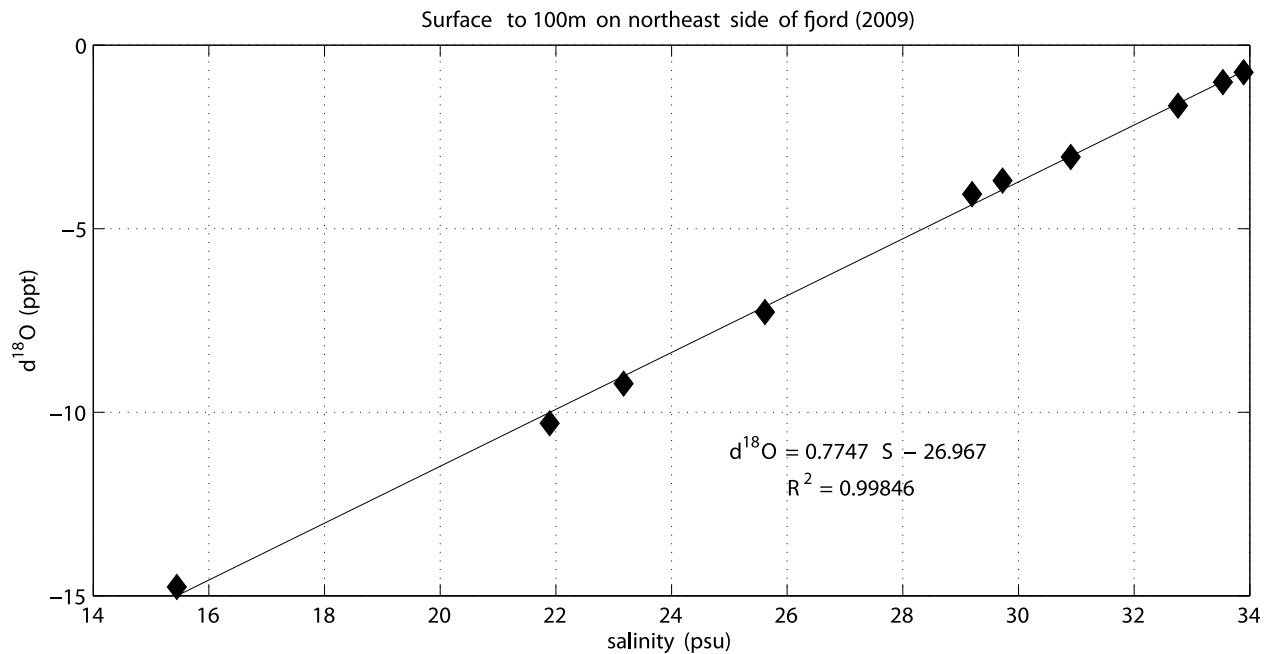
Figure 10. Plot of $\delta^{18}O$ versus salinity measured from bottle samples in the upper 100 m on the northeastern side of the fjord in 2009.

the northeastern side of the fjord in 2009. These data include surface samples taken in the outflowing, fresh plumes discussed in section 6. The data fall on a straight line with an intercept of −27 ppt at zero salinity. This is significantly more negative than typical Arctic river water, indicating that, at least locally, ice shelf melt input signals are discernable. Deep salinity versus $\delta^{18}O$ data (at salinities >33 psu) in Petermann Fjord, Hall Basin, and Robeson Channel to the north also, however, fall on a similar line. Rather than evidence of glacial melt, this is due to the fact that waters entering the Canadian Archipelago from the north inherit a brine signature produced over the Arctic shelves, which pulls the data on a $\delta^{18}O$-S plot down and to the right of a seawater meteoric mixing line (M. B. Alkire et al., Sea-ice melt and meteoric water distributions in Baffin Bay and the Canadian Arctic Archipelago, submitted to *Journal of Marine Research*, 2010). In Petermann Fjord the mixing line connecting Atlantic waters with the Arctic brine happens to extend through the surface data.

6. Surface Survey

[31] On 20 August 2009 a towed CTD survey was conducted across Petermann Fjord from the ship's fast response craft (FRC), with the goal of measuring surface water properties with greater spatial resolution than was possible from the ship, and making measurements both adjacent to the edge of the glacier and close to the fjord walls. Data were collected in real time from an instrument towed at a depth of approximately 1.5 to 2 m and a boat speed of 3 to 4 kts.

[32] Figure 11 shows salinity along the survey track, plotted on top of MODIS satellite data from the preceding day. On the date of the survey itself, the eastern shore of the fjord was packed with large, loose pieces of glacial ice, unlike the apparent large area of open water in this image. Cameras on

the cliff top above (at an elevation of about 900 m (J. Box, personal communication, 2009)) together with observations from the ship, suggest that these pieces were mobile during the day of the survey. In several places along the outer edge of these large yet loose pieces of glacial ice, surface water and small pieces of ice were seen to be moving. There was considerable evidence of surface eddy activity, with clear lines of shear, and brash often aligned in fronts. Ice of deeper draft was seen to move more slowly, if at all, suggesting that motion may have been limited to the upper couple of meters. On the western side of the fjord, which was occupied by small sea ice floes during the survey, a current of about one knot carried small pieces of ice out of the fjord within a few hundred meters of the rock wall.

[33] Background values of salinity during the survey (28–29 psu) were similar to those observed at the surface in Nares Strait, beyond the mouth of Petermann Fjord. Significantly fresher water than this was observed in three locations toward the start of the survey. The first was close to the edge of the fjord, in a region of obvious surface flow both away from and toward the ice on small scales. The second was in the entrance to a small cove formed by large loose pieces of glacial ice. Satellite imagery suggests that the third relatively fresh outflow was located between the loose pieces of ice and the original, unbroken ice front. Salinity was almost constant at >29 psu across the central portion of the glacier, dropping to 28.5 psu and exhibiting more variability once the survey track turned the corner to head in along the fjord. Surface drainage off the glacier was apparent in many places throughout the survey, but did not seem to have any obvious impact on local salinity.

[34] The localized and shallow nature of the fresh water plumes observed suggests that these likely result from surface melt which has drained off the glacier and subsequently been dammed behind loose pieces of ice. While surface melt
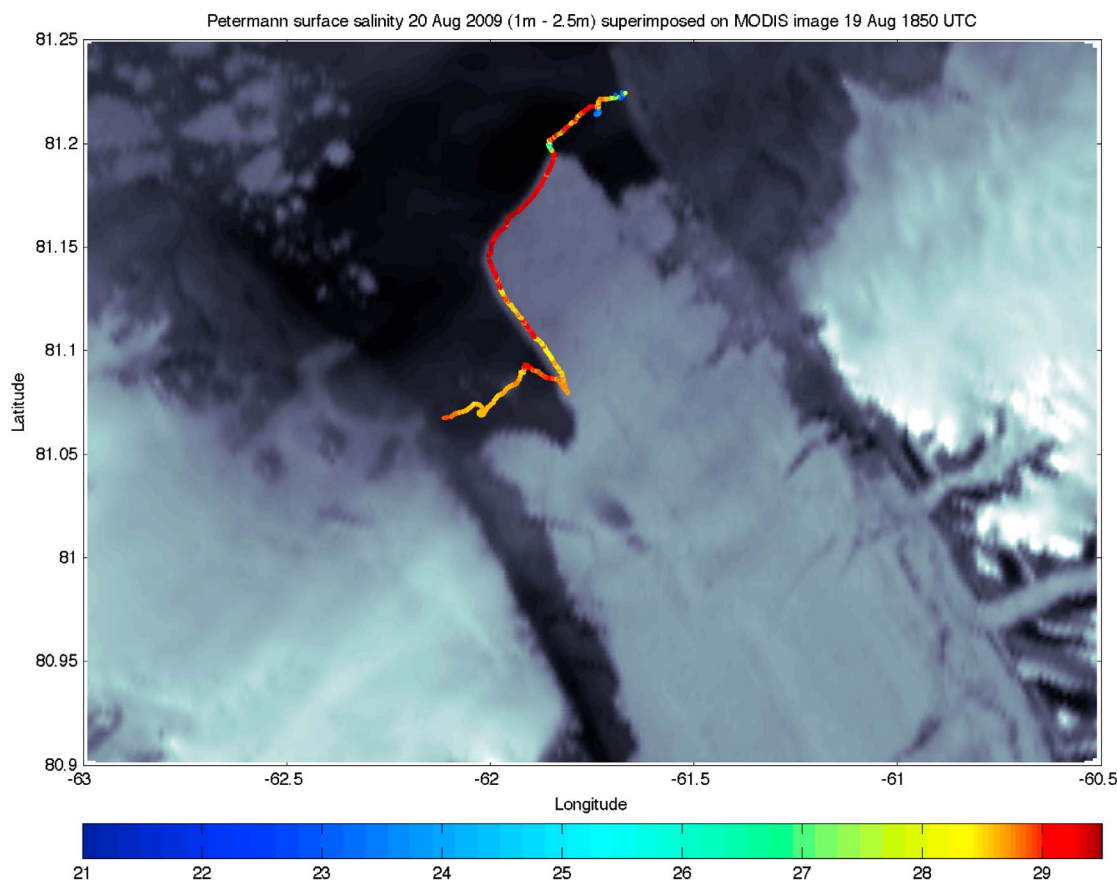
Figure 11. Salinity at 1–2.5 m during a towed CTD survey conducted on 20 August 2009. The background MODIS data are from 1850 UTC on 19 August 2009. Note that the dark band along the north east side of the ice tongue is ice-free water, but the dark band on the south west side is the shadow cast far out over the shelf by the 900 m cliffs that border it.

is thought to account for only a very small fraction of the glacier's total mass loss, an understanding of its episodic release from under the ice shelf may help us to better constrain estimates of surface ablation (currently based on the surface energy budget at a single location on the ice shelf and over only a short period in time [*Rignot and Steffen*, 2008]).

7. Discussion

7.1. Under Ice Water Mass Structure

[35] Estimates of the rate of bottom melting, made from the divergence in radar-based measurements of ice discharge [*Rignot and Steffen*, 2008] and assuming steady state conditions, suggest that Petermann ice shelf undergoes much of its melting within 20 km of its grounding line, over which distance it thins from 600 m to approximately 200 m. At the ice front, the thickness is 50–60 m.

[36] Ice thickness measurements made by *Rignot and Steffen* [2008] also show that the Petermann ice shelf exhibits pronounced under-ice topography, with deep channels in the underneath of the ice running parallel to the fjord over much of its length. CTD data collected by *Rignot and Steffen* [2008] beneath the ice shelf at a location approximately 15 km from the grounding line on the northeastern side of the fjord, in the crest of one of these under-ice channels, is plotted in θ-S space in Figure 12 (yellow) together with CTD data from each of our three surveys in the fjord. (Note that the through-ice CTD data published by *Rignot and Steffen* [2008] and reproduced here were calibrated by scaling the conductivity such that the deep θ-S characteristics matched those measured by our well-calibrated CTD cast near the ice front in 2003.) The slope of the through-ice [*Rignot and Steffen*, 2008] data is indicated; note that it is Gade like with a value of 2.35 between 135 m and approximately 500 m, below which the slope shallows to match that in the deeper portion of all of the CTD profiles measured within and outside the fjord.

[37] The schematic in Figure 13 illustrates the picture which emerges of the water mass structure under the Petermann ice shelf:

[38] 1. The deep water of the fjord below the 500 m depth of the grounding line is fairly uniform in properties over depth. At any given depth, however, Petermann Fjord properties are distinct from those in Hall Basin, suggesting episodic renewal of the fjord deep water via spill over from
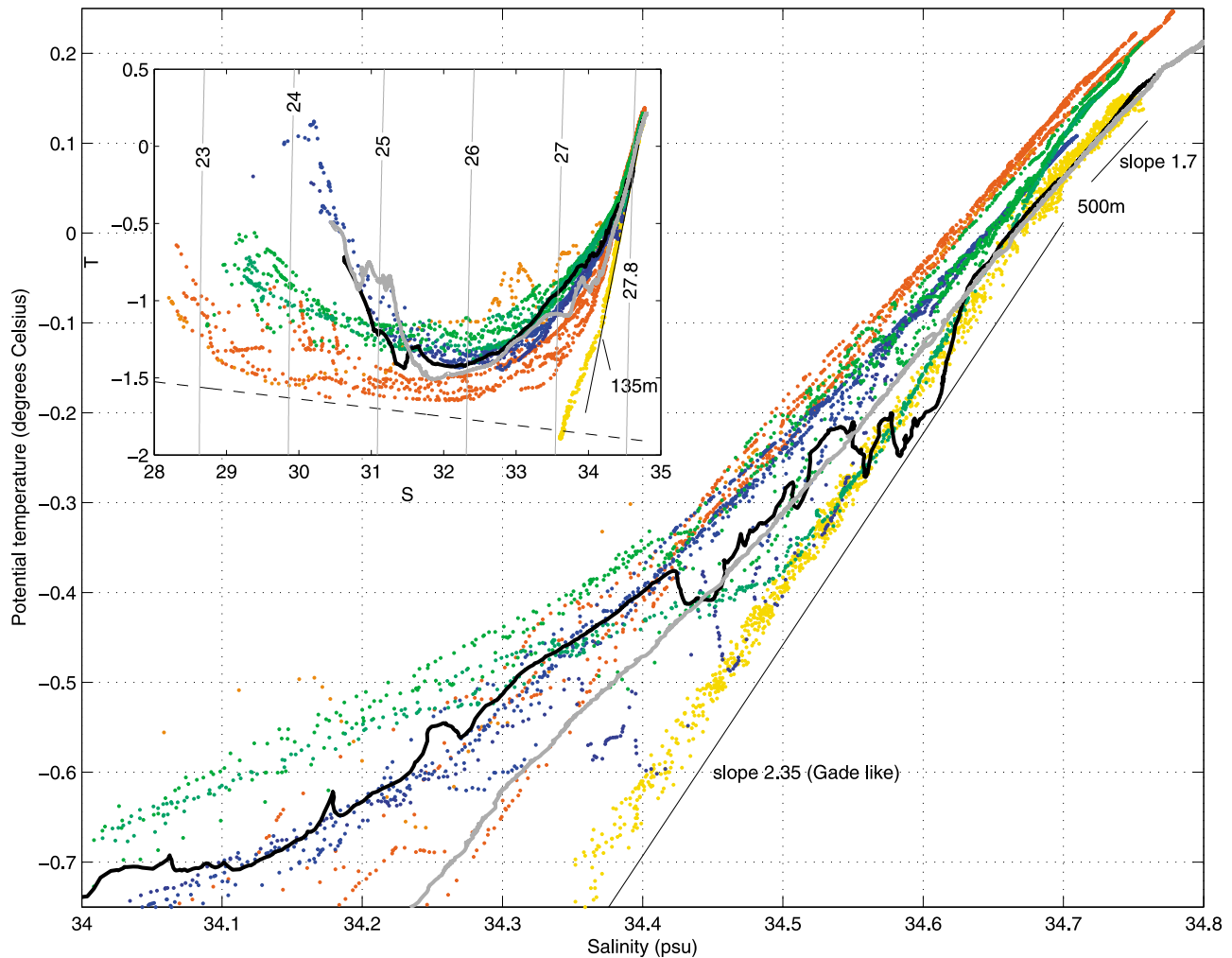
Figure 12. Potential temperature versus salinity plot illustrating many of the data discussed in the text. Plotted in yellow is the through-ice CTD data from *Rignot and Steffen* [2008]. The 2009 CTD section data are shown in green (with the three northeastern profiles in dark green) and the 2007 CTD section data are shown in blue (with the northeastern profile in dark blue). Red indicates profiles taken in 2009 outside Petermann Fjord and to the south, lying in a section across Nares Strait (the easternmost of these profiles is shown in orange). The single deep vertical profile taken in the center of the fjord in 2003 is plotted in black, with the corresponding profile for Hall Basin outside the fjord plotted in grey. The slope of the *Rignot and Steffen* [2008] through-ice data is indicated; at middepths, northeastern profiles from 2007 and 2009 exhibit the same slope. The inset shows the same data over the full range of potential temperature and salinity sampled, with potential density contours and the zero pressure freezing line indicated.

the sill. The change in deep water properties between surveys evident in Figures 12 and 4 indicates that such renewal events may occur relatively frequently. The dynamics governing the flow through Nares Strait may therefore be critical to determining the water masses (and amount of heat) that are able to enter the fjord.

[39] 2. Between approximately 180 and 500 m on the northeastern side of the fjord a "Gade-like" slope in θ-S is evidence of mixing between the modified Atlantic water found in Nares Strait with glacial melt water that has formed due to ice-ocean interaction directly beneath the floating ice shelf. In 2009 this mixture was observed in more than one CTD profile, over a distance of approximately 2 km from the northeast shore of the fjord. In 2007, the northeastern CTD profile exhibits interleaving of water masses (between depths of approximately 200 and 270 m) one of which lies on a Gade line (see Figure 12). The full depth profile in the center of the fjord in 2003 also exhibits interleaving of Gade-like water at similar depths. Water that lies below sill depth yet above 600 m appears to be the least ventilated within the fjord, as evidenced by its relatively low dissolved oxygen and high nutrient content. On the southwestern side of the fjord, properties between 180 and 500 m are indistinguishable in θ-S space from those in northern Kennedy Channel, south of the fjord mouth. The geostrophic circulation suggests that there is inflow into the fjord here.
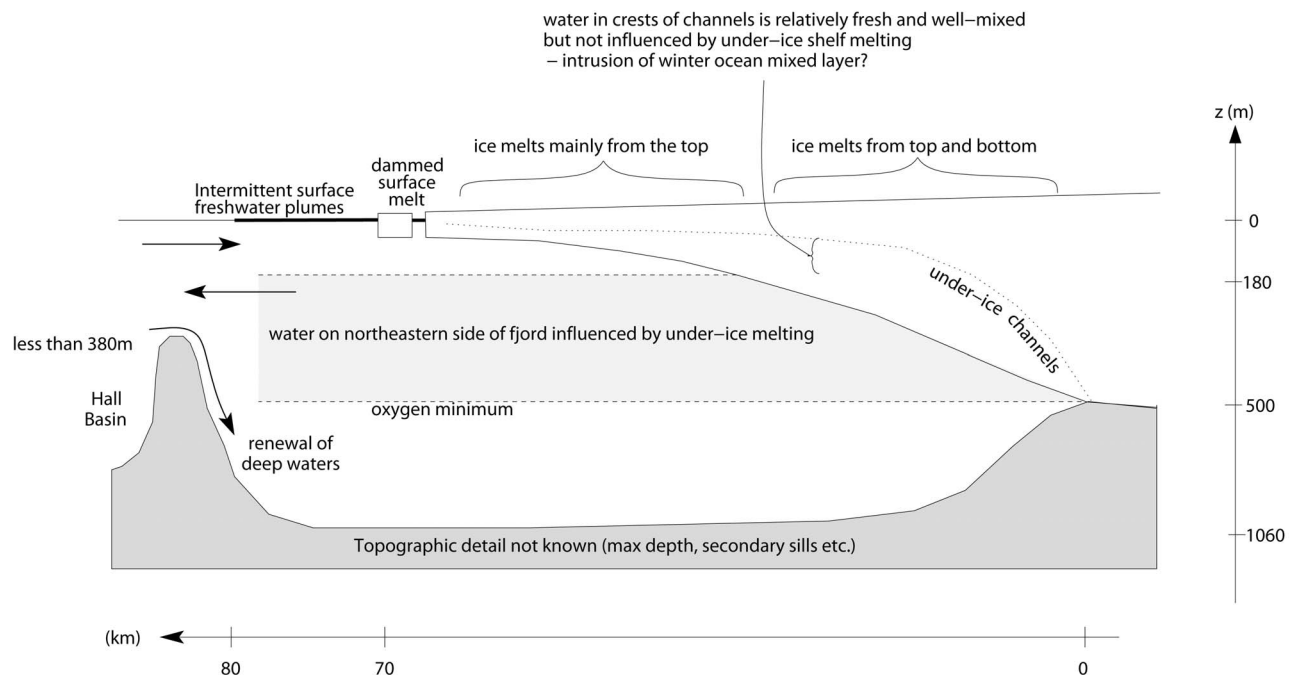
Figure 13. Schematic illustrating the distribution of water masses in Petermann Fjord in the vertical versus along-fjord plane. Note that the circulation is in fact three-dimensional, at least on the scale of the fjord, and possibly also on the scale of the under-ice shelf furrows identified by *Rignot and Steffen* [2008]. Also note that following the major calving event in 2010 the distance from grounding line to ice front is now approximately 55 km.

[40] 3. Through-ice CTD profiles taken by *Rignot and Steffen* [2008] 15 km downstream of the grounding line on the northeastern side of the fjord show a well-mixed and relatively fresh (33.6 psu) layer, approximately 50 m thick, immediately beneath the ice (see magenta curves in Figure 4). The top of the under-ice channel in which these measurements were made is at 60 db. This layer is not the result of under-ice shelf melting, since it does not lie on a Gade line. It may be influenced by a different source of melt water; possibilities include surface melt that has drained through the ice shelf, or melt water from beneath the terrestrial portion of the glacier, added to the ocean at its grounding line and buoyant enough to remain attached to the underneath of the ice shelf within the channel. Perhaps more likely is that this water is an intrusion of the winter (under sea ice) mixed layer in Nares Strait. It is clear from the inset to Figure 12 that the under-ice shelf θ-S correlation for depths shallower than about 135 m is a straight line implying mixing between two end members, one on the Gade line and the other on the freezing line at 33.6 psu. Moorings deployed over several years in Nares Strait demonstrate that there is ample water at the freezing temperature with a salinity of 33.6 psu during the winter. This winter surface ocean mixed layer has a base somewhere between 100 and 135 m, allowing for intrusion under the ice shelf and into the channels noted by *Rignot and Steffen* [2008]. Once beneath the ice shelf, the water is simply cooled slightly to the pressure-adjusted freezing temperature due to contact with ice at 60 db.

[41] 4. Intermittent surface freshwater plumes are apparent near the ice front in the upper few meters, likely due to the release of surface melt or runoff that has collected, trapped by its buoyancy, in under-ice basins or between fractured chunks of the ice shelf, particularly along the northeast shore (see section 7.3).

[42] Density is dominated by salinity at the temperatures observed within Petermann Fjord, and the salinity profiles shown in Figure 4 can therefore also be thought of as profiles of density. The relatively low density of the intruding surface mixed layer discussed above effectively blocks the rising plume of denser melt-influenced "Gade" water, forcing it to detach from the bottom of the ice shelf, such that we would not expect to see any signature of under-ice shelf meltwater above the base of the winter mixed layer in Nares Strait (i.e., above 100–135 m). This is broadly consistent with what we observe at the mouth of the fjord.

7.2. Fresh Water and Heat Fluxes

[43] Since Petermann glacier's ice shelf is approximately 16.6 km wide at its terminus, thins from 600 m to approximately 50 m over its 70 km length, and advances by about 1130 m yr^{-1}, the net fresh water flux out of the fjord that has arisen due to glacial melting beyond the grounding line must be approximately 327 m^3 s^{-1} or 0.327 mSv.

[44] To melt ice at −20°C (a deliberately low, conservative estimate) at this rate would require a heat flux from the ocean of $Q = \rho V(L + c_p \Delta T) = 1.1 \times 10^{11}$ W. Here $\rho = 917$ kg m^{-3} is the mean density of the ice, $L = 333.55$ kJ kg^{-1} is the latent heat of fusion and $c_p = 2.05$ kJ kg^{-1} K^{-1} is the specific heat capacity of ice. Assuming the ice shelf melting occurs entirely due to heating from below an average heat flux to the shelf of 97 W m^{-2} is required.

[45] Estimates of the heat flux into (and freshwater flux out of) the fjord require measurements of temperature, salinity and velocity along a section at its mouth. While we do not have measurements of the absolute velocity, here we use the snapshot of geostrophic velocity shown in Figure 7 to estimate the fluxes of heat and freshwater across the section. Note that we do not expect the flow to be geostrophic near the surface or the side walls of the fjord and we view these fluxes as first-order estimates.

[46] The geostrophic heat flux Q is

$$Q = \int_A \rho_0 \, c_p (T - T_f) u_g \, dA, \qquad (1)$$

where A is the area of the section, $\rho_0 = 1027$ kg m^{-3} is a reference density, $c_p = 3986$ J kg^{-1} K^{-1} is the specific heat capacity of water, u_g is the along-fjord component of geostrophic velocity, perpendicular to the section, and T_f is the local freezing point, a function of both salinity and pressure. Using the geostrophic velocity field in Figure 7, which includes a uniform barotropic inflow of 3.2 cm s^{-1} such that there is no net volume flux across the section [*Montgomery*, 1974], we find a net heat flux over the 500 m deep CTD section of Q = 3.1 × 10^{11} W, directed into the fjord. At least in summer, when our data was collected, there is ample heat flowing into the fjord to melt Petermann ice shelf.

[47] The geostrophic freshwater flux F is given by

$$F = \int_A \left(1 - \frac{S}{S_0}\right) u_g \, dA, \qquad (2)$$

where $S_0 = 34.76$ psu is a reference salinity, representative of the modified Atlantic water at depths of 200–500 m that interacts with the bottom of the ice shelf. Using the same compensated geostrophic velocity field, we obtain a value for F of 2640 m^3 s^{-1} or 2.6 mSv. Approximately 1 mSv of this flux occurs below 50 m. Note that this net freshwater flux is directed out of the fjord, and is not sensitive to the exact value of S_0. It is considerably bigger than the average freshwater input to the fjord from the melting glacier, due to other sources of freshwater including terrestrial runoff and sea ice melt, and perhaps also because it is a summer snapshot. Note that no extrapolation to the fjord edges has been carried out, and that this represents only the geostrophic portion of the freshwater flux.

[48] Compensating the baroclinic outflow across the 2009 CTD section with a barotropic inflow spread instead over either the full depth of the fjord (assuming negligible change in properties below 500 m) or over only the upper 350 m can change the heat and freshwater flux estimates above by up to a factor of two. However, in both of these extreme cases the heat flux remains larger than the long-term mean required to effect the basal melting, and the freshwater flux remains significantly larger than the ice lost.

[49] Notice that most of the geostrophic outflow from the fjord on its northeastern side occurs higher up in the water column than the Gade-like region influenced by meltwater that has formed beneath the ice shelf. The meltwater fraction $(1 - \frac{S}{S_0})$ in the Gade-like region on the northeastern side of the fjord varies from 0.7% at 185 db to zero at 400 db. If this concentration of glacial melt were to extend over the 6 km of the section closest to its northeastern end, the geostrophic

flux of freshwater exiting in this region, stemming from under-ice melting, would be approximately 0.05 mSv. Even this generous estimate of glacial melt output is almost an order of magnitude too small to account for the meltwater produced by the ice shelf.

[50] Clearly, the fate of the fresh water produced by under-ice melting of Petermann glacier close to its grounding line is not as simple as a geostrophically trapped outflow on the northeast side of the fjord. Nor does the freshwater appear to exit at the surface as part of a simple 2-D estuarine circulation. It is likely that variability of both the velocity field and the freshwater content with time plays a significant role. Covariance between the flow and the salinity at tidal frequencies, for example, can generate a mean freshwater flux that our snapshot surveys would not properly represent. The dynamic response of the fjord circulation to local and remote surface wind forcing during the mobile ice season, too, will impact annually averaged fluxes. Strong katabatic winds appear to blow along the fjord, which may generate episodic upwelling of warmer subsurface waters close to the ice shelf front. During our 2009 survey such wind events released surface meltwater, as well as discharging large, loose pieces of the ice shelf into Nares Strait.

[51] Sea ice is also likely to be important. In most recent years there has been open water in the mouth of the fjord for only a couple of months, limiting the water mass transformation that can occur due to sea ice formation. The lid of fast ice present throughout much of the year will moderate the effects of wind stress and air-sea heat exchange. In neighboring Nares Strait, very different flow regimes are observed in fast and mobile ice seasons [*Rabe et al.*, 2010], and we have no reason to expect the circulation in Petermann Fjord to resemble our mobile ice summer snapshots throughout the whole year.

7.3. Constraints on Melting and Calving

[52] The melt rate of Petermann glacier reaches a maximum of 25 m yr^{-1} at a distance approximately 10 km downstream of its grounding line [see *Rignot and Steffen*, 2008, Figure 1]. The surface melt rate is estimated at only about 1 m yr^{-1}, implying that the majority of this melting must be due to heating of the ice shelf by the comparatively warm, modified Atlantic water that impinges on it. The temperature of the water incident on the bottom of the ice shelf, at depths shallower than the grounding line, therefore has the potential to be important in determining the melt rate, thickness profile and calving point. Whether basal melting responds linearly to changes in ocean temperature depends on the specific ice-ocean boundary layer mechanisms governing ocean heat extraction, which are at present poorly known.

[53] However, melting of the ice shelf does not seem to be limited by the amount of heat entering the fjord, with more heat currently available than is required to effect the observed melting (see sections 3 and 7.2). Furthermore, while the melt rate of the glacier drops off to near zero 30 km downstream of the grounding line [*Rignot and Steffen*, 2008, Figure 1], with ice thickness decreasing only very gradually from that point on, the calving front is a further 40 km downstream. These observations suggest that
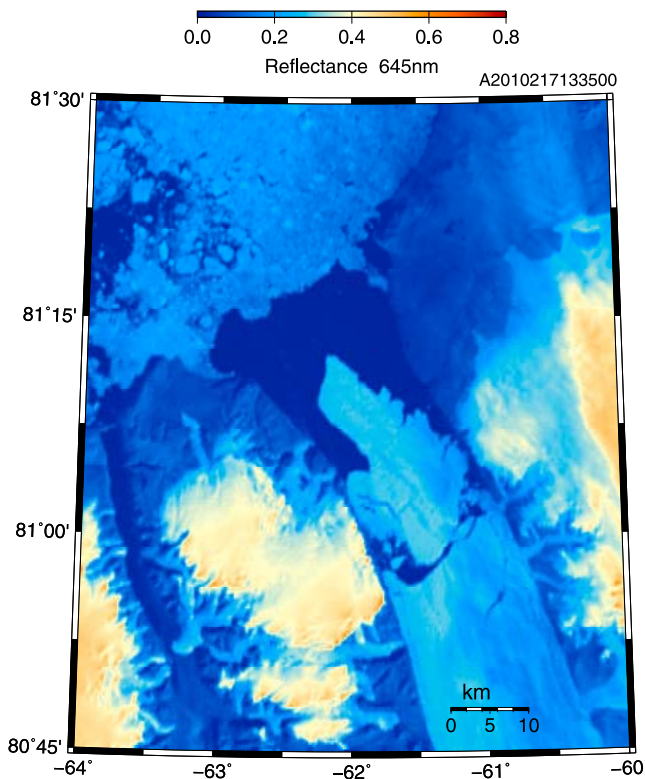
Figure 14. MODIS Aqua data from 1335 UTC on 5 August 2010 showing the ice island which calved from Petermann's floating ice shelf.

other factors, yet to be determined, besides oceanic heat input must also play a role in controlling the melt rate.

[54] Calving is presently a small term in the ice mass balance of Petermann's ice shelf, although what determines its magnitude, as well as the position of the calving front, is unclear. Calving may be limited by the amount of energy available from wind and tide to flex the ice sheet and apply stresses at its grounding line. The tidal range at the ice front is of order 2–3 m, and tidal flexing of the ice shelf about a hinge line close to the grounding line has been observed using satellite radar interferometry [*Rignot*, 1996]. Due to the limited fetch and geographic setting, wave energy transmitted to the ice is likely to be small compared with that available to ice shelves on the Antarctic peninsula (where long wavelength infragravity waves have been implicated in ice shelf collapse [e.g., *Bromirski et al.*, 2010]). Wave energy at shorter wavelengths is in turn dependent on sea ice cover, which may provide a damping. Sea ice can also delay the escape of glacial ice from the fjord once it has calved.

[55] An alternative hypothesis is that the calving position is determined by the fjord geometry. Petermann Fjord narrows from 21 km at the glacier's grounding line to about 15 km at its 2009 terminus. This geometry may make it difficult for ice to escape via calving until the fjord starts to widen again and the lateral pressure is reduced, perhaps not coincidentally at the location of the 2003–2009 ice front. The shear against the side walls, together with the additional

pressure imposed by inflowing subsidiary glaciers on the northeast side of the fjord, creates zones of fractured ice along the edges, which seem to calve first, often leaving a central tongue (as in 2009, see Figure 11), which is subsequently particularly vulnerable. Both walls of the fjord rise in dramatic, vertical cliffs near the ice front, perhaps eroded by ice pressure at the water line. The ice shelf, at the same time, collects and transports the debris from rock falls out of the fjord.

[56] As discussed in section 7.1, the presence of relatively buoyant, cold, intruding winter mixed layer water beneath the ice shelf forces the rising plume of Gade-like, melt-influenced water to detach from the bottom of the ice shelf, and prevents melting from occurring higher in the water column. This suggests that oceanic influence on the thickness of the ice shelf is reduced when the base of the ice rises above the base of the ocean winter mixed layer at approximately 100 m depth. Subsequent thinning of the ice shelf will be controlled by the surface energy balance on top of the ice and, if the 1 m yr^{-1} surface melt rate measured by *Rignot and Steffen* [2008] is typical of the entire ice shelf, will amount to a taper of approximately 1 m in every 1 km. This small thickness change is roughly what the ice thins by over its final 20 km [*Rignot and Steffen*, 2008]. Does the ice, then, thin to the minimum achievable by oceanic heat transfer long before reaching its terminus, and yet remain too thick to calve?

[57] Changes in the winter mixed layer depth may therefore be important; this is set by the depth of convective mixing beneath growing sea ice, and hence is intimately linked to the wintertime sea ice conditions in Nares Strait and perhaps even the Lincoln Sea.

7.4. Recent Major Calving

[58] On 4 or 5 August 2010 a substantial portion of Petermann's floating ice tongue (measuring 253 ± 17 km^2 and with a volume of approximately 12 km^3) calved to form an ice island (Figure 14) which has subsequently been tracked as it has broken up and made its way southward toward Baffin Bay. The calving event has attracted significant attention, in part due to the possibility of a positive feedback on the retreat of Petermann glacier, associated with the fact that it is grounded significantly below sea level. If Petermann glacier were to speed up and thin as a result of any change in the buttressing by its ice shelf, its retreat would take the grounding line into deeper, rather than shallower, ground. Such a feedback has recently resulted in the rapid loss of the entire floating shelf at Jakonshavn Isbrae further south [*Holland et al.*, 2008], with associated surging of the land-based portion of the glacier (and implications for sea level).

[59] While the recent calving of Petermann glacier has resulted in a shorter ice tongue than ever previously observed (Falkner et al., submitted manuscript, 2010b), the volume calved is small in terms of the glacier's mass balance (equivalent to approximately 1 year's supply of ice to the shelf across the grounding line [*Rignot and Steffen*, 2008]) and there is no evidence as yet of an associated change in flow rate. Stable glaciers can calve infrequently and irregularly, and whether the recent event is indicative of a change from Petermann's previously stable regime [*Joughin et al.*, 2010] has yet to be determined.

[60] Interestingly, the change in ice front position may feed back on the circulation and water mass properties within the fjord. The data presented here provide a baseline against which such change may be assessed.

7.5. The Future

[61] The data in hand are insufficient to establish conclusively what determines the position of the calving front, and the net melt rate of Petermann glacier. As such, the relative importance of the factors outlined in section 7.3 for the future of Petermann glacier is unclear. Associated with anthropogenic climate change we might expect a change in the ocean temperature at the sill of the fjord, as well as considerable change in the sea ice extent, but the impact of such changes on glacial melt and calving rates is far from evident.

[62] Warmer incident Atlantic waters may increase basal melting and thinning over the 20 km of the ice shelf closest to its grounding line. Further discussion of the source of the Atlantic water present at the mouth of the fjord, and possible changes in incident water mass properties, is the subject of a forthcoming publication. A transition to drift ice (rather than fast ice) conditions in Nares Strait during the winter would provide the opportunity for more net sea ice growth and hence a deeper intruding winter mixed layer, potentially reducing the impact of basal melting on the ice shelf.

[63] Current heavy sea ice conditions keep surface temperatures in the mouth of the fjord low throughout the year. Ice-free conditions in summer would allow surface temperatures to rise, although this direct effect of insolation is unlikely to extend deep enough (60 m) to warm the water that is positioned to move under the ice shelf. Changing sea ice conditions in both summer and winter may also affect the amount of wave energy incident on the ice front, potentially altering calving rates. Surface ablation rates may be expected to change in a globally warmer world, as might the flow rate of the ice shelf.

[64] Note that there is variability in the forcing of the ice shelf on all timescales, and that this may be considerably larger than any secular trend associated with anthropogenic climate change.

8. Conclusions

[65] Petermann glacier in the north west of Greenland drains about 6% of the Greenland ice sheet. It is one of only four major outlet glaciers that are grounded well below sea level, and one of only two of these that retain a substantial floating ice shelf. Radar and satellite based thickness estimates suggest that the ice shelf loses at least 80% of its mass through basal melting. Based on the results of three opportunistic ocean sampling efforts in Petermann fjord in August 2003, 2007, and 2009, we have attempted to characterize the fjord-scale oceanography and from it infer the under-ice shelf water mass structure, heat flux available to melt the ice, and fate of the resulting melt water. To our knowledge these are the first substantial oceanographic measurements to be made in Petermann Fjord.

[66] Our bathymetric measurements illustrate that the more than 1000 m deep fjord is separated from neighboring 800 m deep Hall Basin by a substantial sill; hydrographic constraints combined with the limited bathymetry data

suggest that the depth of this sill lies between 350 and 450 m. Modified Atlantic water with a temperature close to 0.2°C and a salinity of 34.77 psu flows over the sill and episodically renews the deep waters of the fjord. The frequency of such renewal events is unclear; tracer data suggests that the deeper parts of the fjord are relatively isolated, while the difference in water mass properties between surveys in the upper 500 m of the water column implies a much shorter renewal timescale.

[67] On the north east side of the fjord, and in the depth range 200 m to at least 500 m, the water close to the ice front exhibits a temperature-salinity relationship and dissolved oxygen content characteristic of ice shelf basal melting by sea water. During our surveys in August 2007 and August 2009, subsurface geostrophic flow out of the fjord over the northeastern half of the section was compensated by inflow on the southwestern side of the fjord. Tidal currents at semidiurnal frequency are of the same magnitude as the geostrophic flow, and reduce by a factor of two below about 50 m. There is evidence from remote sensing for a cyclonic circulation at the surface in the mouth of the fjord. The flow structure is fundamentally three dimensional on at least the scale of the fjord, and perhaps even the scale of the under-ice channels identified by *Rignot and Steffen* [2008].

[68] $\delta^{18}O$ tracer data, while somewhat ambiguous due to the complicating effects of larger-scale regional processes, indicates the presence of glacial melt water in the upper portion of the water column. Dissolved oxygen suggests that the water below sill depth yet above the depth of the glacier's grounding line is the oldest in the fjord, supporting the idea of renewal of deep water via spillover at the sill with subsequent lifting of middepth waters.

[69] Localized freshwater plumes have been observed at the surface, reaching salinities as low as 15 psu. Rather than the result of basal melting, these are thought to arise due to surface melt which has drained off (or through) the ice shelf and subsequently become dammed by under-ice topography or behind loose pieces of ice. Strong katabatic wind events blowing out of the fjord, such as that prior to our sampling in 2009, cause loose pieces of glacial ice characteristic of the north east wall of the fjord to be discharged, with the release of any dammed buoyant water.

[70] The net heat flux into the fjord implied by our geostrophic section is three times as large as that required to cause the observed melting of glacial ice. Although this is based on a summer snapshot, 3 year long temperature time series in Nares Strait suggest that water mass properties at sill depth do not exhibit large seasonal variability. We therefore conclude that Nares Strait supplies ample heat to the fjord throughout the year to accommodate the implied melt rates.

[71] Fresh water fluxes are harder to interpret. The total net geostrophic freshwater flux across our hydrographic section is an order of magnitude greater than that arising due to glacial melt, as one might expect given the prevalence of other fresh water sources in the region. However, the freshwater flux over that portion of the section apparently influenced by glacial melt is an order of magnitude too small. Temporal variability and storage are no doubt important, preventing us from conclusively establishing the

fate of the basal melt water using the snapshot surveys reported here.

[72] Our results indicate that, while the ice shelf may be sensitive to the temperature of modified Atlantic water entering the fjord, other factors such as ocean winter mixed layer depth, mobile versus land fast sea ice cover, and fjord geometry may also be important. Heat input cannot be assumed to be the limiting factor. A targeted and sustained observational campaign is required to provide a definitive answer to the question of what determines the melt rate and calving frequency/location. Combined with an ocean and ice modeling effort, this would allow us to more confidently assess the impact of future forcing changes in the region on Petermann glacier and its floating tongue.

References

Bessels, E. (1876), *Scientific Results of the United States Arctic Expedition, Steamer Polaris, C. F. Hall Commanding*, vol. 1, *Physical Observations*, 86 pp., US Gov. Print. Off., Washington, D. C. (Available at http://www.archive.org/details/cu31924029881095.)

Bromirski, P. D., O. V. Sergienko, and D. R. MacAyeal (2010), Transoceanic infragravity waves impacting Antarctic ice-shelves, *Geophys. Res. Lett.*, *37*, L02502, doi:10.1029/2009GL041488.

Copland, L., D. R. Mueller, and L. Weir (2007), Rapid loss of the Ayles ice shelf, Ellesmere Island, Canada, *Geophys. Res. Lett.*, *34*, L21501, doi:10.1029/2007GL031809.

Das, S. B., I. Joughin, M. D. Behn, I. M. Howat, M. A. King, D. Lizarralde, and M. P. Bhatia (2008), Fracture propagation to the base of the Greenland ice sheet during supraglacial lake drainage, *Science*, *320*, 778–781.

Gade, H. G. (1979), Melting of ice in sea water: A primitive model with application to the Antarctic ice shelf and icebergs, *J. Phys. Oceanogr.*, *9*, 189–198.

Higgins, A. (1991), North Greenland glacier velocities and calf ice production, *Polarforschung*, *60*, 1–23.

Holland, D. M., R. H. Thomas, B. D. Young, M. H. Ribergaard, and B. Lyberth (2008), Acceleration of Jakobshavn Isbrae triggered by warm subsurface ocean waters, *Nat. Geosci.*, *1*, 659–664.

Joughin, I., B. E. Smith, I. M. Howat, T. Scambos, and T. Moon (2010), Greenland flow variability from ice-sheet-wide velocity mapping, *J. Glaciol.*, *56*, 415–430.

Melling, H., Y. Gratton, and G. Ingram (2001), Ocean circulation within the North Water polynya of Baffin Bay, *Atmos. Ocean*, *39*(3), 301–325.

Melling, H., et al. (2008), Fresh-water fluxes via Pacific and Arctic outflows across the Canadian polar shelf, in *Arctic-Subarctic Ocean Fluxes*, edited by R. R. Dickson, J. Meincke, and P. Rhines, pp. 193–261, Springer, Dordrecht, Netherlands.

Montgomery, R. B. (1974), Comments on "Seasonal variability of the Florida Current" by Niiller and Richardson, *J. Mar. Res.*, *32*, 533–534.

Münchow, A., and H. Melling (2008), Ocean current observations from Nares Strait to the west of Greenland: Interannual to tidal variability and forcing, *J. Mar. Res.*, *66*, 801–833.

Münchow, A., H. Melling, and K. K. Falkner (2006), An observational estimate of volume and freshwater flux leaving the Arctic Ocean through Nares Strait, *J. Phys. Oceanogr.*, *36*, 2025–2041.

Münchow, A., K. Falkner, and H. Melling (2007), Spatial continuity of measured seawater and tracer fluxes through Nares Strait, a dynamically wide channel bordering the Canadian Archipelago, *J. Mar. Res.*, *65*, 759–788.

Padman, L., and S. Erofeeva (2004), A barotropic inverse tidal model for the Arctic Ocean, *Geophys. Res. Lett.*, *31*, L02303, doi:10.1029/2003GL019003.

Parkinson, C. L., and D. J. Cavalieri (2008), Arctic sea ice variability and trends, 1979–2006, *J. Geophys. Res.*, *113*, C07003, doi:10.1029/2007JC004558.

Rabe, B., A. Münchow, H. Johnson, and H. Melling (2010), Nares Strait hydrography and salinity field from a three-year moored array, *J. Geophys. Res.*, *115*, C07010, doi:10.1029/2009JC005966.

Rignot, E. (1996), Tidal motion, ice velocity and melt rate of Petermann Gletscher, Greenland, measured from radar interferometry, *J. Glaciol.*, *42*, 476–485.

Rignot, E., and P. Kanagaratnam (2006), Changes in the velocity structure of the Greenland ice sheet, *Science*, *311*, 986–990.

Rignot, E., and K. Steffen (2008), Channelized bottom melting and stability of floating ice shelves, *Geophys. Res. Lett.*, *35*, L02503, doi:10.1029/2007GL031765.

Rignot, E., M. Koppes, and I. Velicogna (2010), Rapid submarine melting of the calving faces of west Greenland glaciers, *Nat. Geosci.*, *3*, 187–191.

Serreze, M. C., M. M. Holland, and J. Stroeve (2007), Perspectives on the Arctic's shrinking sea-ice cover, *Science*, *315*, 1533–1536.

Shepherd, A., and D. Wingham (2007), Recent sea-level contributions of the Antarctic and Greenland ice sheets, *Science*, *315*, 1529–1532.

Straneo, F., G. S. Hamilton, D. A. Sutherland, L. A. Stearns, F. Davidson, M. O. Hammill, G. B. Stenson, and A. Rosing-Asvid (2010), Rapid circulation of warm subtropical waters in a major glacial fjord in east Greenland, *Nat. Geosci.*, *3*, 182–186, doi:10.1038/NGEO764.

Zwally, H. J., W. Abdalati, T. Herring, K. Larson, J. Saba, and K. Steffen (2002), Surface melt-induced acceleration of Greenland ice-sheet flow, *Science*, *297*, 218–222.

K. K. Falkner, College of Oceanic and Atmospheric Sciences, Oregon State University, 104 COAS Administration Bldg., Corvallis, OR 97331-5503, USA.

H. L. Johnson, Department of Earth Sciences, University of Oxford, South Parks Road, Oxford OX1 3AN, UK. (helen.johnson@earth.ox.ac.uk)

H. Melling, Institute of Ocean Sciences, Department of Fisheries and Oceans, 9860 W. Saanich Rd., Sidney, BC V8L 4B2, Canada. (humfrey.melling@dfo-mpo.gc.ca)

A. Münchow, College of Earth, Ocean and Environment, University of Delaware, 112A Robinson Hall, Newark, DE 19716, USA.